

Computer simulations of polyelectrolyte stars and brushes

This article has been downloaded from IOPscience. Please scroll down to see the full text article.

2008 J. Phys.: Condens. Matter 20 494221

(<http://iopscience.iop.org/0953-8984/20/49/494221>)

View [the table of contents for this issue](#), or go to the [journal homepage](#) for more

Download details:

IP Address: 129.252.86.83

The article was downloaded on 29/05/2010 at 16:45

Please note that [terms and conditions apply](#).

Computer simulations of polyelectrolyte stars and brushes

Christos N Likos¹, Ronald Blaak and Aaron Wynveen

Institute for Theoretical Physics II: Soft Matter, Heinrich-Heine-University of Düsseldorf,
Universitätsstraße 1, D-40225 Düsseldorf, Germany

E-mail: likos@thphy.uni-duesseldorf.de

Received 23 July 2008, in final form 20 August 2008

Published 12 November 2008

Online at stacks.iop.org/JPhysCM/20/494221

Abstract

We briefly review results pertaining to the conformations, interactions and phase behavior of two related soft matter systems: star-branched polyelectrolytes and spherical polyelectrolyte brushes. Moreover, we present new results on the complexation of stars with oppositely charged, spherical, hard colloids, demonstrating the versatility of these systems to form novel complexes that result in a variety of patchy colloids, whose morphology can be affected by small amounts of added salt. Finally, we demonstrate that spherical polyelectrolyte brushes with low grafting density have distinct characteristics from dense brushes as regards the condensation of counterions. Here, condensation of counterions takes place along the rods and the brush conformation seems to be much more robust to added salt than that of star polyelectrolytes.

(Some figures in this article are in colour only in the electronic version)

1. Introduction

Star-shaped polymer aggregates are a very important class of macromolecules in chemistry, soft matter physics and materials science. Their common characteristic lies in the fact that the presence of the soft polymer corona surrounding the colloidal particle on which the chains are grafted or adsorbed acts as a soft potential energy barrier that prevents close approaches by other such macromolecules. In this sense, they bear close resemblance also to self-organized block-copolymer micelles and they can be thought of as strongly curved polymer brushes—the planar brush lying on the other end of the spectrum as far as curvature is concerned. The conformation of the polymer corona and its size and softness as well as the ensuing interaction between the star-shaped particles depend on a number of parameters: the aggregation number or functionality f of the star, the solvent conditions that determine the effective monomer interactions, the chain length N , the grafting density Σ and, in the case of charged stars, also the total charge Q_s of the macromolecule and the salinity of the solution.

Whereas neutral stars are now rather well understood as a result of many efforts in the last 25 years [1–10], less is known about their charged counterparts, termed *polyelectrolyte stars* and abbreviated as PE-stars in what follows. PE-stars

are always to be found in aqueous solvents, since their polar nature is the physical reason for the dissociation of ionizable groups from the chains' backbone, bringing about the charges on the arms and the appearance of counterions in the solution. Typical polyelectrolytes employed in chemically synthesized PE-stars are sodium-sulfonated polystyrene (NaPSS) [11] and polyacrylic acid [12]. Quite often, PE-stars are obtained by self-association of micelle-forming block copolymers [13–15], and their charge and conformations can be influenced by changing the pH of the solution [16, 17].

A system closely related to PE-stars is spherical PE-brushes [18]. Here, the size of the colloidal particle, R_c , on which the PE-chains are grafted is of the order of the brush height, L_0 , or bigger. PE-stars are recovered in the limit $R_c \ll L_0$, whereas crew-cut brushes result in the opposite limit $R_c \gg L_0$, and planar brushes for $R_c \rightarrow \infty$. In all cases, the grafting density Σ that describes the area of the surface per grafted chain as well as the ratio of the distance between grafting points, a , to the brush height L_0 are additional important parameters. The subject and literature of spherical PE-brushes are very rich; here we mention as an example an intriguing and currently topical issue of research, namely the spectacular collapse of the height of densely grafted brushes under the influence of multi-valent counterions [19–22].

The purpose of this paper is to bring forward two *novel* and *distinct* aspects in the field of PE-stars and brushes that have

¹ Author to whom any correspondence should be addressed.

received relatively little attention, and yet they contain exciting new physics and possess high potential for applications. First is the *complex formation* or *complexation* between PE-stars and oppositely charged colloids, which is the subject of section 2. Here, we will demonstrate that a very rich variety of complex morphologies is possible, opening the way for the self-assembly of complex colloids. Second is the issue of the conformations of *sparse* PE-brushes composed of stiff, double-stranded DNA polyelectrolytes (ds DNA) grafted on colloidal particles, a system that shows quite different force–distance characteristics than dense brushes. This is discussed in section 3. Finally, in section 4 we summarize and draw our conclusions.

2. Polyelectrolyte stars

2.1. Conformations and interactions in the bulk

There are three physical parameters characterizing PE-stars: their degree of polymerization N , their functionality f and the charging fraction $0 \leq \alpha \leq 1$, representing the fraction of monomers that carry an elementary charge $+e$.² The conformations of high-functionality PE-stars have been studied extensively by Borisov and Zhulina, employing scaling theory [23, 24], and by Klein Wolterink *et al* [25], who employed self-consistent field theory. The salient characteristics of PE-stars in salt-free solutions are the stretching of the arms, which attain a rodlike shape, and the absorption of the vast majority of counterions in their interior. Recently, Shusharina and Rubinstein extended the scaling theory for PE-stars to *arbitrary* concentrations and salinities [26]. As far as the conformation of a single star is concerned, they established that the relevant dimensionless parameter governing the star shape is the ‘coupling constant’:

$$\zeta \equiv \lambda_B \frac{fN\alpha}{R_s}, \quad (1)$$

where R_s is the PE-star radius and $\lambda_B = e^2/(\epsilon k_B T)$ is the Bjerrum length in a solvent of dielectric permittivity ϵ at absolute temperature T with Boltzmann’s constant k_B . The case $\zeta < 1$ corresponds to very weakly charged stars, for which no counterion condensation in the star interior occurs, whereas in the regime $\zeta > 1$ the arms become stretched and counterions are absorbed within the star interior. In fact, the arm stretching, which amounts to a swelling of the stars, can be thought of as being caused by the high osmotic pressure of the counterions in the star interior, a property that justifies the term *osmotic stars*.

Jusufi *et al* have followed a different strategy by employing molecular dynamics (MD) computer simulations and introducing a variational free energy for PE-stars with $f \gtrsim 10$ and relatively high charging fractions, $\alpha = 1/6, 1/4$ and $1/3$ [27, 28]. The osmotic regime was recovered, witnessed by a strong arm stretching ($R_s \sim N$), with monomer density profiles $c(r) \sim r^{-2}$ as functions of the distance r from the star center and strong counterion condensation. It is indeed straightforward to check that the stars considered in [27, 28]

fulfil the $\zeta > 1$ criterion of Shusharina and Rubinstein [26]: since the radius R_s of the same scales as $R_s \propto \sigma N$, σ being the monomer length [27, 28], one obtains $\zeta \cong \lambda_B f \alpha / \sigma \cong f$, given that both σ and λ_B are microscopic length scales³. Evidently, ζ exceeds unity by at least an order of magnitude for high-functionality stars. An additional feature of the work of Jusufi *et al* [27, 28] was the separation of the absorbed counterions into two states, the Manning-condensed ones, cylindrically trapped in the neighborhood of the rods, and the spherically condensed ones, which float within the PE-star.

The variational free energy of Jusufi *et al* has been generalized to *two* PE-stars held at center-to-center distance D and yields an effective interaction $V_{\text{eff}}(D)$, whose validity is amply confirmed by comparison with simulations [27, 28]. The theory is based on the assumption of *no interdigitation* between the arms from different PE-stars as the two approach each other, in full agreement with both simulation results and ideas put forward in the pioneering work of Pincus [29]. The no-interdigitation assumption has indeed been shown to be valid even in the semi-dilute regime for the $\zeta \gg 1$ -stars of concern here [26]. The PE-star effective interaction $V_{\text{eff}}(D)$ is ultrasoft in nature and caused mainly by the entropy of the trapped counterions [27–29]. On the basis of $V_{\text{eff}}(D)$, the phase diagram of PE-star solutions has been drawn [30], showing crystallization into fcc- and bcc-phases for sufficiently high functionalities f and partially confirmed in the experimental study of Furukawa and Ishizu [12]. Though the validity of the pair potential approximation in the high concentration regime for which some of the crystals in the phase diagram appear [30] can be put in question [26], estimates of the strength of three-body forces in concentrated PE-star solutions show that these are weak [31]. The effect of salt is to both shrink the stars and to weaken their mutual repulsions [28].

2.2. Complexation of polyelectrolyte stars with colloids

When PE-stars are brought in confinement close to *planar* and *neutral* walls, they maintain their ability to capture most of their counterions, despite their strong deformation there [32]. The effective PE-star–wall force is now caused not only by the aforementioned entropy loss of the counterions due to confinement but also by a chain-compression mechanism when the star–wall distance approaches the star radius R_s . This star–wall repulsion has been generalized to curved walls, i.e. neutral colloids of radius $R_c > R_s$, by means of a Derjaguin-like approximation, showing that the star–colloid repulsions drive a demixing transition at sufficiently high concentrations [33].

A much richer subject is that of the behavior of PE-stars close to charged walls and, in particular, walls that carry a charge *opposite* to that of the star and may lead to an attachment of the latter on the wall surface, i.e. to complexation of the star. Though the complexation of polyelectrolyte *chains* with oppositely charged surfaces or colloids has been the subject of intensive research in the last

³ In aqueous solutions, $\lambda_B = 7.2 \text{ \AA}$, which is of the same order as the monomer length. Charged systems in organic solvents are rare and in this case the argument holds even more strongly, since λ_B is larger by as much as an order of magnitude due to the much lower dielectric constant of organic materials.

² Without loss of generality, we treat the chains as polycations.

few years by theory, simulations and experiments [34–53], the complexation of PE-stars has only recently attracted attention. Motivated by the intriguing shapes that PE-stars [16, 17] and charged microgels [54–56] assume when adsorbed on mica plates, Konieczny and Likos recently studied the adsorption characteristics of multiarm PE-stars ($f = 10, 18, 30$ and 50) on oppositely charged walls [57]. A variety of five distinct star conformations has been discovered, with narrow crossover regimes between these. This opens up the way for the control of surface functionalization by PE-stars and even dynamical switching between different states by modification of the surface potential or the pH of the solution.

The case of PE-star complexation on spherical colloids introduces additional parameters into the problem. Now, apart from f and the star radius R_s and charge Q_s , the colloid charge Q_c and radius R_c enter the formulation of the problem. Results from computer simulations involving a single PE-star and a single colloid show that the morphologies of star-colloid complexes strongly resemble those between stars and planar walls [57], but the location of transitions between these depends sensitively on the size ratio R_s/R_c , in particular for $R_s/R_c > 1$. These results will be the subject of another publication [58]. Here, we turn our attention to the case of complexation of more than one PE-star on the colloid, which is very promising in opening up possibilities to self-assemble a novel kind of *patchy colloids* [59, 60].

To this end, we employ MD simulations using a simplified, yet semi-realistic, model that contains all essential features: a single star with functionality f arms, formed by a central core to which f polymer chains of length N are connected. It is assumed that all the monomers that constitute the polymers are identical in showing a mutual short-range repulsive interaction, modeled by the Weeks–Chandler–Andersen (WCA) or shifted Lennard-Jones potential

$$v_{\text{WCA}}(r) = \begin{cases} 4\epsilon \left[\left(\frac{\sigma}{r}\right)^{12} - \left(\frac{\sigma}{r}\right)^6 + \frac{1}{4} \right] & r \leq 2^{1/6}\sigma \\ 0 & r > 2^{1/6}\sigma, \end{cases} \quad (2)$$

where σ is the effective diameter of the particles and the energy ϵ fixes the temperature to $T = 1.2\epsilon/k_B$ via the Boltzmann constant k_B . The connectivity between neighboring monomers within the chain is maintained by the standard finite extension nonlinear elastic (FENE) potential [61]

$$v_{\text{FENE}}(r) = \begin{cases} -\frac{1}{2}k_{\text{FENE}} \left(\frac{R_0}{\sigma}\right)^2 \ln \left[1 - \left(\frac{r}{R_0}\right)^2 \right] & r \leq R_0 \\ \infty & r > R_0, \end{cases} \quad (3)$$

in which a spring constant $k_{\text{FENE}} = 7\epsilon$ ensures that the maximum separation between bonded monomers can not exceed $R_0 = 2\sigma$. The interactions with the core of a star are similar, except that the core is larger and has a hard-core radius $R_d = 2\sigma$ from which the interactions with the monomers emanate. This leads to a short-range repulsion of the form

$$v_{\text{WCA}}^c(r) = \begin{cases} \infty & r \leq R_d \\ v_{\text{WCA}}(r - R_d) & r > R_d, \end{cases} \quad (4)$$

and a binding between the first monomer of each polymer chain with the core

$$v_{\text{FENE}}^c(r) = \begin{cases} \infty & r \leq R_d \\ v_{\text{FENE}}(r - R_d) & r > R_d. \end{cases} \quad (5)$$

Note that the chains do not have fixed sites, but are free to redistribute over the surface of the core.

A fraction $\alpha = 1/3$ of the monomers, distributed in a periodic fashion along the chains, carries a monovalent charge $+e$, which is balanced by an equivalent number of counterions with charge $-e$, but interacting otherwise as the monomers within the arms of the star. The Coulomb interaction between the charges reads as

$$\beta v_{\text{Coul}}(r) = \lambda_B \frac{Z_i Z_j}{r}, \quad (6)$$

with $Z_i = \pm 1$ the valency of a particle, $\lambda_B = 7.2 \text{ \AA}$ the value of the Bjerrum length corresponding to water at room temperature and $\beta = (k_B T)^{-1}$. The Coulomb potential acts between all charged species in the system, including the star's and colloid's own counterions as well as any additional salt co- and counterions present.

We consider here stars with $f = 5$ and $N = 50$, resulting in a total of $Q_s = +85$ elementary charges per star. Under these conditions the equilibrium center-to-end radius of the star (averaged over all arms) in a dilute solution and in the absence of the colloid is $R_s \cong 26\sigma$ [27, 28]. To restrict the search in the parameter space, which includes the colloid and star radii as well as their charges, we fix the colloid radius at the same value as the star's, $R_c = R_s$, and vary the colloidal charge Q_c as well as the salinity. Our system consists of a single colloid and two stars, therefore it makes sense to consider values of $|Q_c|$ not too dissimilar from $2Q_s$. Indeed, for $|Q_c| \ll 2Q_s$ only one star will (partially) complex with the colloid, whereas in the opposite case it is to be expected that additional stars would complex with the colloid, thus simulating only two stars does not lead to the equilibrium configuration. The system was simulated in a cubic box with edge length $L = 120\sigma$ with full periodic boundary conditions employing the Ewald summation technique. In our MD simulations we typically employed a total of 2×10^6 timesteps for equilibration and an additional 6×10^6 timesteps to gather statistics. Here, the timestep was $\Delta t = 0.002\tau_{\text{MD}}$, where $\tau_{\text{MD}} = \sqrt{m\sigma^2/\epsilon}$ denotes the MD time unit for the monomers of mass m . Finally, we employed a Langevin thermostat during the simulation run.

In figure 1, we show a typical equilibrium configuration of the resulting complex for the case $Q_c = -180$, for which the two stars together are not capable of neutralizing the colloid even at full adsorption ($|Q_c| > 2Q_s$). It can be seen that, in the absence of salt (figure 1, left panel), the stars fully adsorb on the colloid on opposite poles and assume on its surface a 'starfish configuration' [57]. The resulting complex is a patchy colloid with positively charged caps on the north and south poles and a negatively charged equatorial region. In a concentrated system, a large number of such patchy colloids will be present and they will feature anisotropic interactions among themselves. We expect that the two adsorbed stars

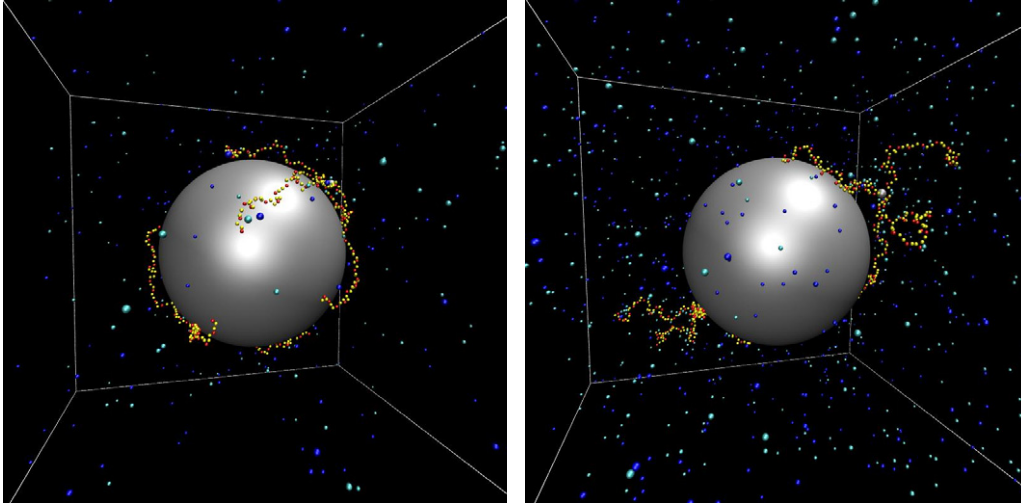


Figure 1. Typical snapshots of an undercharged complex formed by two stars with charge $Q_s = +85$ each, adsorbed on a charged spherical colloidal particle of charge $Q_c = -180$. The light (yellow) and dark (red) balls on the arms denote neutral and charged monomers of the star, respectively. Light (blue) and dark (blue) spheres in the solution are star and colloid counterions (left panel) as well as salt ions (right panel). The big sphere in the middle is the colloidal particle. Left panel: no added salt. Right panel: with 0.03 M of added salt.

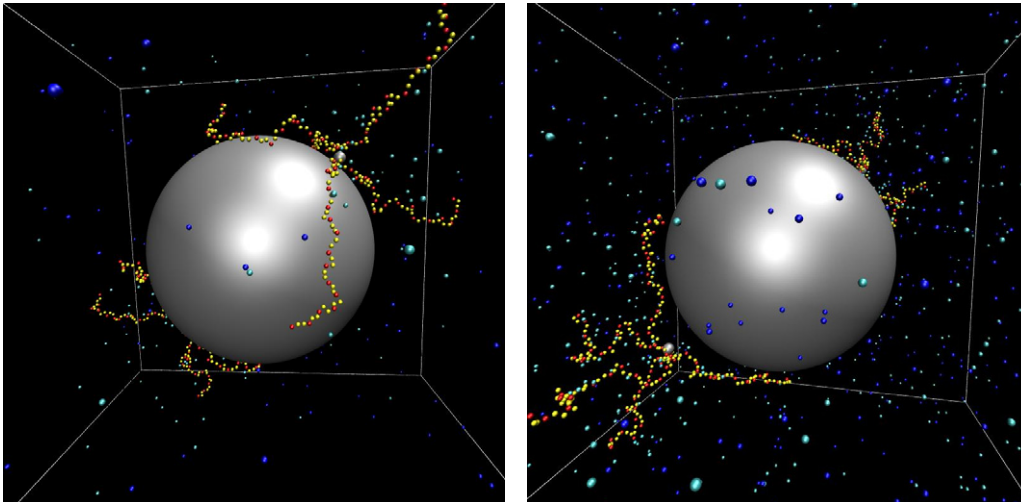


Figure 2. Same as figure 1 but for a colloidal charge $Q_c = -120$. The PE-chains are denoted light grey (yellow) and the counterions as grey spheres.

on the poles will fluctuate around their positions on the approach of a similar patchy colloid but they will maintain their diametrically opposite locations on average. However, at variance with the currently popular models for patchy colloids for which patches *attract* each other [59, 60], here we have the opposite case: patches will repel each other and they will be attracted to the equatorial regions of other complexes. On these grounds, we call the new complexes *inverse patchy colloids*. We anticipate that under the right conditions of Q_c , Q_s and size ratios, complexes with different numbers of patches and arrangements will self-assemble in a mixture.

The form of the patches can be tuned by added salt. As can be seen in figure 1, right panel, a salinity of 0.03 M is already sufficient to cause significant detachment of the stars from the colloidal surface. The resulting star conformations are now more akin to the ‘anemone configuration’ in the terminology of [57]. In this fashion, the location of the center-of-charge of

the stars with respect to the fixed colloid center as well as the distribution of the positive charge in the polar regions can be tuned by salt. We anticipate that further increase of the ionic strength of the solution will lead to a breakup of the complex.

In figure 2 we show the situation when the colloid carries a charge $Q_c = -120$, so that $|Q_c| < 2Q_s$ in this case. The first striking feature, seen in figure 2, left panel, is that we now obtain an *overcharged* or *charge-reversed* complex, since the two stars that are now adsorbing are more than sufficient to compensate the colloidal charge. At the same time, the adsorption is now considerably weaker than in the case $Q_c = -180$ studied before. At all times, two to four chains are not attached on the colloid. The remaining ones, however, are strongly attached to it, so that the stars assume now the ‘anemone configuration’ [57]. It is worth noting that although the salt-free, $Q_c = -120$ case ends up showing a similar type of distribution of the star distance from the colloid center

as the $Q_c = -180$ case with added salt (see figure 3), the star conformations are quite different between the two cases. Finally, addition of salt for the case $Q_c = -120$ (figure 2, right panel) leads, as expected, to a very significant detachment of the stars from the colloidal surface. Here, only one or two star chains remain attached to the colloid, while the rest extends into the solution.

The probability distribution $P(D)$ of finding a star center at distance D from the colloid is shown in figure 3 and corroborates the results presented above. In particular, it can be seen that the addition of salt pushes the stars away from the colloid and enhances the fluctuations of their positions. Systematic investigations on the types of complexes, on their characterization and on coagulation kinetics are currently underway.

3. Polyelectrolyte brushes

3.1. Previous results

Polyelectrolyte brushes result when the charged chains are grafted on a colloidal sphere whose size is at least comparable with the height of the grafted polymer. Apart from solvent quality, additional parameters that affect the brush conformation here are the salinity, the pH that controls the amount of charge on the chains and the grafting density Σ , defined as $\Sigma = f/(4\pi r_s^2)$, r_s being the radius of the colloidal sphere. With $a \equiv \Sigma^{-1/2}$ denoting the average distance between grafting points, the ratio a/L plays an important role in determining the brush monomer profile, L being the unperturbed polymer size. For $a \ll L$ one speaks of a dense brush and the case $a \gtrsim L$ corresponds to sparse brushes. Recently, the effects of grafting density on the conformations of neutral polymer brushes have been analyzed by means of Monte Carlo simulations [62], establishing a crossover from the well known parabolic brush profile [63–65] to a fully stretched regime as $a/L \rightarrow 0$. For PE-brushes, on the other hand, the aforementioned ratio is not a sufficient parameter to describe the brush conformation; as we will establish shortly, at least in the sparse brush regime $a/L \cong 1$, the absolute value of L is also relevant.

Recently, Fazli *et al* [66] conducted a computer simulation study of planar PE-brushes consisting of rodlike (i.e. stiff) PE-chains of length L , varying the ratio a/L and monitoring the dependence of the brush height $L_0/L \leq 1$ on this ratio and on counterion valency. For sparse brushes and monovalent counterions a decrease of the brush height with a has been found, following the law $L_0/L - (1/2) \sim a^{-2}$, whereas in the dense-brush limit, $a \rightarrow 0$, L_0 approaches L from below. The brushes considered in [66] featured PE-rods with full rotational flexibility at their grafting points on the surface.

For dense brushes, a theory has been proposed [67] that generalizes the theory of effective interactions for PE-stars [27, 28], and which considers exclusively the contributions from the entropy of the condensed counterions as two brushes approach. In this approach, the entropic effective interaction between two spherical brushes at surface-to-surface

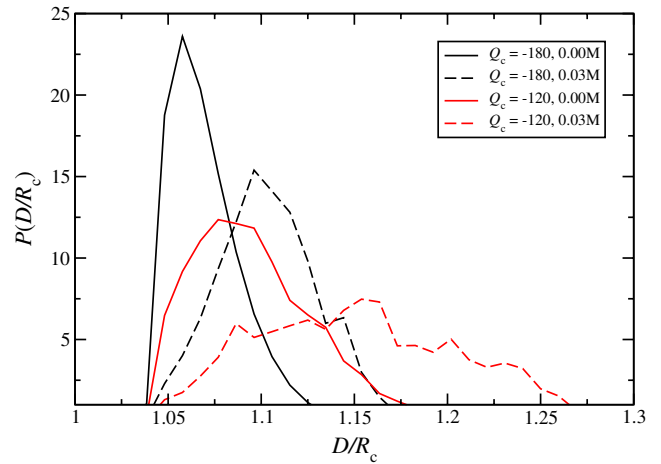


Figure 3. The probability distribution $P(D)$ of the distance D separating the colloid and the core of the stars for two colloid charges $-120e$ (overcharged) and $-180e$ and without and with 0.03 M salt. The averages are taken over both stars.

distance D vanishes for $D > 2L_0$, and for $0 \leq D \leq 2L_0$ reads as

$$\beta V_{\text{en}}(D) = N_{\text{trap}} \left[\frac{y}{2RK} \ln^2 \left(\frac{y}{2R} \right) + 2R_c \left(\frac{2}{RK} - \frac{1}{L_0} \right) \ln \left(\frac{r_s}{R} \right) + \ln \left(\frac{2L_0}{RK} \right) \right], \quad (7)$$

where $y \equiv (D + 2r_s)$, $K = 1 - 2r_s/R + x(1 - \ln x)$, $x = y/(2R)$, N_{trap} represents the number of spherically trapped ions, and $R = r_s + L_0$. A similar shape was found by Dubois *et al* for the related case of polyelectrolyte-coated colloids [68].

In a recent paper [69], Kegel *et al* measured both the structural characteristics (brush height and its dependence on ionic strength) and the force–distance dependence between sparse spherical PE-brushes, employing a sophisticated and sensitive optical-tweezer apparatus that featured an accuracy of 1 pN for the forces and 3 nm for the separation. The grafted polyelectrolyte employed in [69] was stiff, double-stranded DNA (ds DNA). A subsequent theoretical analysis of a large collection of data [70] revealed that the dense-brush expression for the force–distance dependence derived from equation (7) above, $F_{\text{en}}(D) = \partial V_{\text{en}}(D)/\partial D$, fails to account for the experimental data. Instead, a different physical mechanism giving rise to the brush–brush repulsion was put forward. On the basis of the fact that the brushes are sparse and the chains have a rodlike shape, it has been argued that the forces arise due to mutual compression [32] of the ds DNAs of each brush against the surface of the opposing colloidal sphere. This results in a new expression for the effective brush–brush interaction, $V_c(D)$, whose validity has been amply confirmed by direct comparison with experimental data and reads as [70]

$$\beta V_c(D) = \frac{(Z_{\text{eff}}N)^2 \lambda_B}{D} \left\{ 2 \ln \left(\frac{D}{d} \right) + \left(\frac{D}{L_0} \right)^3 \left[\ln \left(\frac{L_0}{d} \right) - 1 \right] \right\}. \quad (d \ll D \leq L_0) \quad (8)$$

In equation (8) above, d is the diameter of the grafted chains ($d = 18 \text{ \AA}$ for ds DNA) and Z_{eff} is a fit parameter that

describes the net charge per monomer (or per chain) resulting from the partial compensation of the bare DNA charge through counterion condensation. Typical values of Z_{eff} turn out to lie in the range of 10% [70], a value that reasonably agrees with the degrees of compensation found for PE-stars [27, 28]. Nevertheless, this value along with other characteristics of the brush that have been taken as input in the theory of [70] on the basis of experimental evidence (brush height and orientation of chains to the surface) should be analyzed on the basis of a realistic simulation model. We have performed such detailed simulations and present our approach and results below.

3.2. The simulation model

The spherical DNA polyelectrolyte brush is modeled as a large, neutral sphere of radius r_S with f chains of N charged monomers (beads), with radius r_{DNA} , each grafted at one end to the colloidal sphere. Counterions with radius r_{C+} are added to maintain charge neutrality in the implicit-solvent system, and, in some simulations, salt is also included. The short-ranged excluded volume interactions of the DNA beads, the counterions, and the salt ions, as well as of the large colloidal sphere, are described by shifted/truncated Lennard-Jones potentials, assuming good solvent conditions.

$$V_{\text{LJ}}^{\alpha\beta}(r) = \begin{cases} 4\varepsilon_{\text{LJ}} \left[\left(\frac{\sigma_{\text{LJ}}}{r - r_{\alpha\beta}} \right)^{12} - \left(\frac{\sigma_{\text{LJ}}}{r - r_{\alpha\beta}} \right)^6 + \frac{1}{4} \right], & r \leq 2^{1/6}\sigma_{\text{LJ}} + r_{\alpha\beta} \\ 0, & r > 2^{1/6}\sigma_{\text{LJ}} + r_{\alpha\beta} \end{cases} \quad (9)$$

where $\varepsilon_{\text{LJ}} = 1.0 \text{ kJ mol}^{-1}$ and $\sigma_{\text{LJ}} = 4.0 \text{ \AA}$.⁴ Such a potential was applied to each component of the system so that the potentials at the surfaces of every object were identical, independent of the object's size, where $\alpha, \beta = \text{S, DNA or } C+$, the latter denoting the counterions. In particular, $r_{\alpha\beta} = (r_\alpha + r_\beta) - \sigma_{\text{LJ}}$ with $r_{C+} = (1/2)\sigma_{\text{LJ}}$, r_S ranges between 600 and 1300 \AA , and $r_{\text{DNA}} = 9.0 \text{ \AA}$, the approximate radius of the DNA molecule [71]. The mass of each DNA bead was taken to be 660 amu (1 amu = $1.66 \times 10^{-27} \text{ kg}$) [72] and that of a counterion or salt ion as 20 amu.

The DNA chains were grafted to the colloidal surface by tethering the first DNA bead of each chain to fixed locations on the colloidal sphere. These fixed locations initially were determined by placing $f = 100$ charged particles on the sphere and allowing them to distribute themselves uniformly over the sphere to minimize their repulsive electrostatic energy. The first DNA beads and these fixed locations and adjacent DNA beads were bonded via a harmonic potential

$$V_{\text{b-harm}}(r) = (1/2)k_{\text{b}}(r - h)^2 \quad (10)$$

where $h = 3.4 \text{ \AA}$, corresponding to the rise (bond length) between neighboring B-DNA base pairs, and the value of $k_{\text{b}} = 210 \text{ kJ mol}^{-1} \text{ \AA}^{-2}$ was chosen to give a dispersion of $\approx 0.15 \text{ \AA}$ in the rise [73, 74].

⁴ Note that the value of ε_{LJ} employed here is $\varepsilon_{\text{LJ}} = 0.4k_{\text{B}}T$ in thermal units and thus about half of the value employed for the parameter ε for the PE-stars in equation (2).

Stiffness was imposed on the DNA chains by including a harmonic valence angle potential between neighboring bonds

$$V_{\theta\text{-harm}}(\theta) = (1/2)k_{\theta}(\theta - \pi)^2. \quad (11)$$

The value of k_{θ} was varied in the simulations from 0 to 750 kJ mol^{-1} , corresponding to persistence lengths of the charged chains with values ranging from ~ 50 to 1000 \AA . (Note that the charge on the DNA beads and the finite size of the beads also contribute to the rigidity of the chain.)

The chains and counterions also interacted electrostatically. Each DNA bead was given a negative unit charge $-e$. The negative charge of each DNA bead of the brush was offset by a corresponding number of monovalent counterions. The electrostatic potential between the charges was described by the usual Coulomb potential⁵

$$V_{\text{Coul}}(r) = \frac{Z_\alpha Z_\beta e^2}{4\pi\epsilon\epsilon_0 r^2} \quad (12)$$

where $Z_\alpha(Z_\beta)$ is the valency of particle $\alpha(\beta)$, $Z_{\text{DNA}} = -1$ and $Z_{C+} = +1$. Here, we assume that the water solvent can be implicitly treated as a dielectric background with $\epsilon = 80$ and ϵ_0 is the permittivity of free space. In some simulations, salt, described as co-ions (S^-) and counterions (S^+) with the same LJ parameters as the DNA's counterions, was also included. The valencies of the salt cations were varied; values $Z_{S+} = +1, +2$ and $+3$ were considered.

Simulations were carried out in a cubic box with a side length of 4000 \AA and periodic boundaries, the brush situated at the center. Increasing the volume of the box by 50% was found to yield results within the uncertainty of the quantities being measured. Coulombic interactions were computed using the three dimensional version of the Ewald summation method with 'conducting' boundary conditions. The parameters for the Ewald sum were chosen to give a relative error in the computation of the Coulombic interactions of the order of 10^{-6} . The canonical (NVT) ensemble using the Nosé-Hoover thermostat was used, at a temperature $T = 298 \text{ K}$. Initial configurations were chosen with the chains being fully extended with neighboring beads on the chain at their equilibrium bond length and the counterions distributed randomly within 100 \AA of a chain. A typical simulation consisted of $\mathcal{N}_{\text{eq}} \gtrsim 10^5$ equilibration timesteps (2 fs step^{-1}) and $\mathcal{N}_{\text{prod}} \sim 5 \times 10^5$ production steps. A snapshot from a simulation of our model brush is shown in figure 4.

3.3. Results and discussion

The DNA grafting density, the length of the DNA chains, the salt concentration and valency, and the stiffness of the chain were all varied (see table 1), whereas the number of chains was held fixed ($f = 100$), for the individual simulations. We determined a number of quantities, the most relevant for this study being the brush height L_0 and the degree to which counterions or salt ions neutralize the net charge of the brushes.

⁵ In this section and, in particular, in equation (12) we express the Coulomb interaction in the SI system because we have employed SI units in expressing all other energy scales as well.

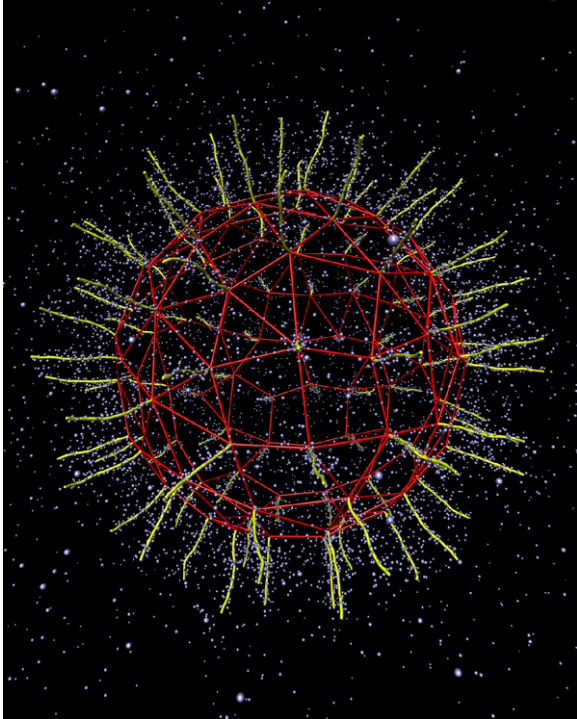


Figure 4. A snapshot of a simulation of a brush with stiff chains after the system has equilibrated. Here, the parameters are $f = 100$, $N = 100$, $\Sigma = 10^{-5} \text{ \AA}^{-2}$, and $k_{\theta} = 750 \text{ kJ mol}^{-1}$. The PE-chains are denoted yellow and the counterions are rendered as gray spheres. Most counterions in the brush are concentrated about the DNA chains.

The former is defined as the distance from the colloid surface at which the normalized chain radial distribution $4\pi r^2 \rho_{\text{DNA}}(r)$ falls to half that of fully extended chains. The effective charge Z_{eff} of the brush was taken to be the ratio of the sum of the charges of those counterions and salt counterions/co-ions within a distance of L_0 of the colloid surface to the absolute charge of the brush. Full neutralization of the brush corresponds to $Z_{\text{eff}} = 0$. This effective charge of the brush is a lower limit because there exists a large counterion concentration in the halo region beyond L_0 , as can be seen in figure 5.

The grafting density was varied by changing the radius of the colloid, keeping f fixed. The principal grafting density studied was 10^{-5} \AA^{-2} , which corresponds, roughly, to a nearest neighbor distance between the grafting points of 340 \AA , the contour length of a fully stretched $N = 100$ -bead chain. As shown in table 1, the height of the brush for these rigid chains increases, to a small extent, for increasing grafting densities, consistent with results of studies of more densely grafted planar PE-brushes [75]. This may be attributed to increased repulsion between the chains because of their closer proximity. With regard to counterion neutralization of the brush, changing the grafting density displayed a similar trend to that of changing the length of the DNA chains, since, for either case, the ratio of the length of the chains to the distance between nearest neighbor grafting points is altered. Fewer counterions were found within the brush for lower grafting

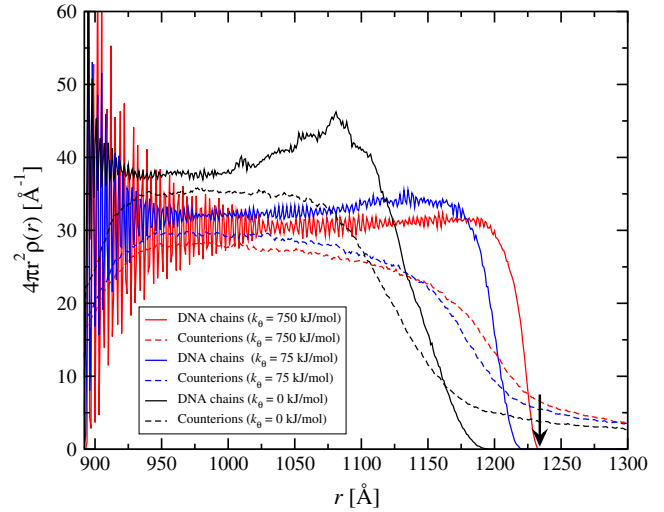


Figure 5. The DNA chain and counterion distributions for spherical brushes with parameters: $f = 100$, $N = 100$, $\Sigma = 10^{-5} \text{ \AA}^{-2}$, $r_S = 892 \text{ \AA}$ and no added salt, for three different values of the chain stiffness. The thick, downwards-pointing arrow marks the location of the brush height for fully extended chains.

Table 1. The brush height L_0 and the effective charge of the brush Z_{eff} due to partial neutralization by counterions for simulations with various chain grafting densities Σ , number of DNA beads N making up a chain, ionic strength I of added salt (valency of cation given in parentheses), and chain rigidities. Uncertainties for L_0 and Z_{eff} in all simulations are $\sim 5 \text{ \AA}$ and 0.005, respectively.

Σ (10^{-5} \AA^{-2})	N	I (mM)	k_{θ} (kJ mol $^{-1}$)	L_0 (\AA)	Z_{eff}
0.5	100	0	750	325	0.247
1.0	100	0	750	329	0.214
2.0	100	0	750	331	0.183
1.0	75	0	750	246	0.262
1.0	50	0	750	163	0.351
1.0	100	0.1 (+1)	750	334	0.171
1.0	100	0.1 (+2)	750	327	0.176
1.0	100	0.1 (+3)	750	330	0.176
1.0	100	0.3 (+1)	750	332	0.142
1.0	100	0.3 (+2)	750	332	0.140
1.0	100	0.3 (+3)	750	332	0.145
1.0	100	0	75	308	0.211
1.0	100	0	0	262	0.205

densities and/or for smaller chains, yielding results similar to those obtained in studies of planar PE-brushes [76].

We also considered the effects of added salt, for two different ionic strengths and monovalent, divalent, and trivalent salt cations. Results are given in terms of the ionic strength, which is defined as $I = \sum_{\alpha} c_{\alpha} Z_{\alpha}^2$, where the sum is carried out over all salt ions of species α of concentration c_{α} and valency Z_{α} . For example, a 3:1 electrolyte contains one-sixth of the concentration of cations as a 1:1 electrolyte with the same ionic strength. Adding salt increased the neutralization of the brush, but no discernible change was observed in the brush height for these very rigid chains. This result as well as the sole dependence of L_0 on the ionic strength I but *not* on the counterion valencies is in agreement with experimental results on the system modeled in our simulations [69, 70].

We further examined the effects of bending rigidity (stiffness) k_θ on the brush shape. As can be seen from table 1, a reduction of the stiffness by a factor of 10 (from $k_\theta = 750$ to 75 kJ mol^{-1}) only reduces the brush height from 325 to 308 Å. Completely switching the bending rigidity off ($k_\theta = 0$) results in a more significant decrease of the brush height ($L_0 = 262 \text{ Å}$ in this case). The ds DNA molecules (which do feature bending rigidity) remain almost fully stretched, and the density profiles $\rho_{\text{DNA}}(r)$, measured from the brush center, follow a r^{-2} -dependence, similar to the one seen for dense PE-stars [27, 28]. In figure 5, the quantity $4\pi r^2 \rho_{\text{DNA}}(r)$ is shown, which displays a characteristically flat profile reminiscent of the shape of the profiles of neutral brushes for very high grafting densities [62]. Even for the case $k_\theta = 0$ (black curve in figure 5), the inner part of the brush is stretched due to electrostatics. Towards the end of the brush, an overshooting of the curve $4\pi r^2 \rho_{\text{DNA}}(r)$ can be seen, caused by enhanced lateral fluctuations of the chains and some weak coiling towards the chain ends.

The counterion profiles shown in figure 5 follow those of the charged monomers on the DNAs but decay more smoothly than the latter as the chain height L_0 is crossed. There is strong counterion condensation in the interior of the brush and, more precisely, close to the DNA chains, as can be discerned from the simulation snapshot in figure 4. The effective charge Z_{eff} turns out to be of the order of 20% and decreasing with added salt and with chain length. This number is already only a factor of 2 higher than the typical Z_{eff} -values employed in [70]. However, the DNA strands employed in the experiments there were longer, thus we expect Z_{eff} to become lower than the 20% value found here and approach the theoretical values of [70]. Moreover, in view of the strong counterion condensation along the DNA strands, it appears more physical to employ in equation (8) not the bare DNA diameter d but a renormalized one, $d_{\text{eff}} > d$, that takes the layer of condensed counterions into account. Effectively, this corresponds to a theoretical value of Z_{eff} necessary to describe the given experimental curves that is *higher* than 10%, again bringing it closer to the values from simulation. Finally, the charge density of the chains used in the simulations, $(1/3.4) e \text{ Å}^{-1}$, was only half of that of real DNA. Upon doubling this value, to match the charge density of DNA and for an $N = 100$, $\Sigma = 10^{-5} \text{ Å}^{-2}$ brush, the simulation yielded a value of $Z_{\text{eff}} = 10\%$. Therefore, the values of Z_{eff} reported in table 1 provide an upper limit for this quantity.

In figure 6 we show the radial distribution functions of the counterions around the DNA charges. They display very similar shapes for all three values of the bending rigidity considered. The curves for $k_\theta = 0$ are higher than those for $k_\theta \neq 0$ because in the former case the same number of counterions has to be accommodated in a brush of smaller height than in the latter.

Finally, we comment on the orientation of the grafted DNA chains with respect to the spherical surface of the colloids, and in particular with respect to the findings of [66], in which a similar system was considered in planar geometry. Similarly to Fazli *et al*, we have considered rigid chains⁶ freely

⁶ The system of [66] can be formally obtained by allowing $k_b \rightarrow \infty$ and $k_\theta \rightarrow \infty$ in equations (10) and (11).

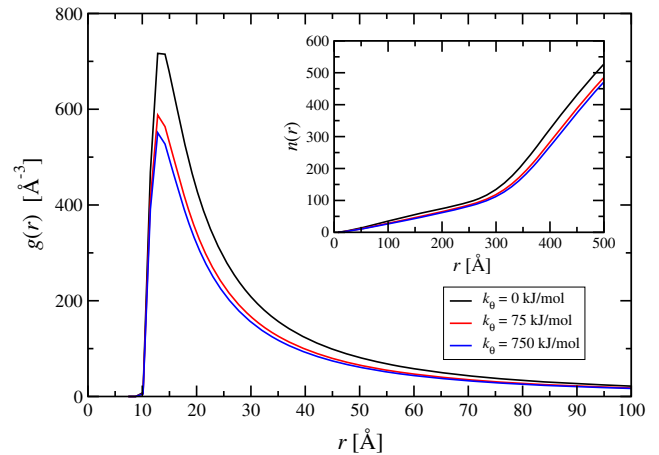


Figure 6. The radial distribution function $g(r)$ of the counterions around a DNA monomer (main plot) and the total number $n(r)$ of counterions within a distance r of the same (inset) for the DNA brushes with parameters as in figure 5.

grafted on a surface. For typical values $a/L \cong 1$, Fazli *et al* found significant deviations of the rods' orientation from the direction perpendicular to the surface, whereas in our case the DNA strands remain at almost perfectly right angles to the surface of the colloid on which they are grafted, despite the fact that there is enough space between the grafting points for them to 'fall flat' on the sphere. The reason for this difference lies in the fact that short rods, $N \cong 10$, were considered in the work of Fazli *et al* [66], but much longer ones, $N = 100$, in this work. The strong electrostatic repulsion between chains is minimized when they all stand vertical to the surface and scales as N^2 with the number of beads. Thus, as N grows, it dominates over the entropy gain from an additional, rotational freedom and keeps the chains not only rigid but also rigidly oriented with respect to the grafting plane. At odds with neutral brushes, the absolute value of the chain length, $L \sim N$, is a relevant parameter, and the conformation cannot be described on the basis of the dimensionless parameter a/L alone.

4. Summary and outlook

We have presented simulation results for two related, charge-polymer-based spherical colloidal particles: ultrasoft star-branched polyelectrolytes and sparsely grafted DNA brushes. The former can aggregate into oppositely charged colloids, building novel forms of complex, patchy colloids, whose self-assembly can be externally steered by the relative charges and sizes of the two components, by the star functionality and by the salt concentration. The latter display a novel form of stabilization force against colloidal coagulation, which is neither strictly steric nor strictly electrostatic in nature. Rather, it can be qualified as a compression force of the stiff DNA strands grafted on the colloids. We have shown that the shape of such brushes is rather insensitive to ionic strength for rigid molecules. Current and planned research is oriented towards a systematic investigation of the control of colloidal patchiness through complexation and the properties of

many-body systems composed of complexes. Further, on the PE-brush system, we are pursuing full simulations of two brushes, with the purpose of measuring the compression-induced forces and analyzing their quantitative characteristics.

Acknowledgments

The authors acknowledge helpful discussions with Arben Jusufi and Martin Konieczny. This work has been supported by the Deutsche Forschungsgemeinschaft. AW wishes to thank the Alexander von Humboldt Foundation for financial support through a Research Fellowship.

References

- [1] Daoud M and Cotton J P 1982 *J. Physique* **43** 531
- [2] Pincus P A and Witten T A 1986 *Macromolecules* **19** 2509
- [3] Witten T A, Pincus P A and Cates M E 1986 *Europhys. Lett.* **2** 137
- [4] Grest G S, Kremer K and Witten T A 1987 *Macromolecules* **20** 1367
- [5] Grest G S, Fetters L J, Huang J S and Richter D 1996 *Adv. Chem. Phys.* **94** 67
- [6] Likos C N, Löwen H, Watzlawek M, Abbas O, Jucknischke O, Allgaier J and Richter D 1998 *Phys. Rev. Lett.* **80** 4450
- [7] Watzlawek M, Likos C N and Löwen H 1999 *Phys. Rev. Lett.* **82** 5289
- [8] Vlassopoulos D, Fytas G, Pakula T and Roovers J 2001 *J. Phys.: Condens. Matter* **41** R855
- [9] Foffi G, Sciortino F, Tartaglia P, Zaccarelli E, Lo Verso F, Reatto L, Dawson K and Likos C N 2003 *Phys. Rev. Lett.* **90** 238301
- [10] Likos C N 2006 *Soft Matter* **2** 478
- [11] Heinrich M, Rawiso M, Zilliox J G, Lessieur P and Simon J P 2001 *Eur. Phys. J. E* **4** 131
- [12] Furukawa T and Ishizu K 2005 *Macromolecules* **38** 2911
- [13] Muller F, Delsanti M, Auvray L, Yang J, Chen Y J, Mays J W, Deme B, Tirrel M and Guenoun P 2000 *Eur. Phys. J. E* **3** 45
- [14] Korobko A V, Jesse W, Egelhaaf S U, Lapp A and van der Maarel J R C 2004 *Phys. Rev. Lett.* **93** 177801
- [15] Korobko A V, Jesse W, Lapp A, Egelhaaf S U and van der Maarel J R C 2005 *J. Chem. Phys.* **122** 024902
- [16] Gorodyska G, Kiryi A, Minko S, Tsitsilianis C and Stamm M 2003 *Nano Lett.* **3** 365
- [17] Kiryi A, Gorodyska G, Minko S, Stamm M and Tsitsilianis C 2003 *Macromolecules* **36** 8704
- [18] Ruhe J, Ballauff M, Biesalski M, Dziezok P, Gröhn F, Johannsmann D, Houbenov N, Hugenberg N, Konradi R, Minko S, Motornov M, Netz R R, Schmidt M, Seidel C, Stamm M, Stephan T, Usov D and Zhang H N 2004 Polyelectrolytes with defined molecular architecture I *Adv. Polym. Sci.* **165** 79
- [19] Santangelo C D and Lau A W C 2004 *Eur. Phys. J. E* **13** 335
- [20] Mei Y, Lauterbach K, Hoffmann M, Borisov O B, Ballauff M and Jusufi A 2006 *Phys. Rev. Lett.* **97** 158301
- [21] Mei Y, Hoffmann M, Ballauff M and Jusufi A 2008 *Phys. Rev. E* **77** 031805
- [22] Ishikubo A, Mays J W, Tirrell M and Div A C S 2005 *Polym. Prepr. Am. Chem. Soc. Div. Polym. Chem.* **46** 27
- [23] Borisov O V and Zhulina E B 1997 *J. Physique II* **7** 449
- [24] Borisov O V and Zhulina E B 1998 *Eur. Phys. J. B* **4** 205
- [25] Klein Wolterink J, Leermakers F A M, Fler G J, Koopal L K, Zhulina E B and Borisov O V 1999 *Macromolecules* **32** 2365
- [26] Shusharina N P and Rubinstein M 2008 *Macromolecules* **41** 203
- [27] Jusufi A, Likos C N and Löwen H 2002 *Phys. Rev. Lett.* **88** 018301
- [28] Jusufi A, Likos C N and Löwen H 2002 *J. Chem. Phys.* **116** 11011
- [29] Pincus P 1991 *Macromolecules* **24** 2912
- [30] Hoffmann N, Likos C N and Löwen H 2004 *J. Chem. Phys.* **121** 7009
- [31] Sadat Khonsari A and Likos C N 2008 unpublished
- [32] Konieczny M and Likos C N 2006 *J. Chem. Phys.* **124** 214904
- [33] Konieczny M and Likos C N 2007 *J. Phys.: Condens. Matter* **19** 076105
- [34] Gurovitch E and Sens P 1999 *Phys. Rev. Lett.* **82** 339
- [35] Mateescu E M, Jeppesen C and Pincus P 1999 *Europhys. Lett.* **46** 493
- [36] Park S Y, Bruinsma R F and Gelbart W M 1999 *Europhys. Lett.* **46** 454
- [37] Nguyen T T and Shklovskii B I 2001 *J. Chem. Phys.* **114** 5905
- [38] Nguyen T T and Shklovskii B I 2001 *J. Chem. Phys.* **115** 7298
- [39] Kunze K K and Netz R R 2000 *Phys. Rev. Lett.* **85** 4389
- [40] Allen R J and Warren P B 2004 *Langmuir* **20** 1997
- [41] Jonsson M and Linse P 2001 *J. Chem. Phys.* **115** 3406
- [42] Jonsson M and Linse P 2001 *J. Chem. Phys.* **115** 10975
- [43] Akinchina A and Linse P 2002 *Macromolecules* **35** 5183
- [44] Dzubiella J, Moreira A G and Pincus P A 2003 *Macromolecules* **36** 1741
- [45] Messina R, Holm C and Kremer K 2003 *Langmuir* **19** 4473
- [46] Holthoff H, Egelhaaf S U, Borkovec M, Schurtenberger P and Sticher H 1996 *Langmuir* **12** 5541
- [47] Behrens S H, Christl D I, Emmerzael R, Schurtenberger P and Borkovec M 2000 *Langmuir* **16** 2566
- [48] Bouyer F, Robben A, Yu W L and Borkovec M 2001 *Langmuir* **17** 5225
- [49] Kleimann J, Gehin-Delval C, Auweter H and Borkovec M 2005 *Langmuir* **21** 3688
- [50] Lin W, Galletto P and Borkovec M 2004 *Langmuir* **20** 7465
- [51] Pericet-Camara R, Papastavrou G and Borkovec M 2004 *Langmuir* **20** 3264
- [52] Dong W F, Ferri J K, Adalsteinsson T, Schönhoff M, Sukhorukov G B and Möwald H 2005 *Chem. Mater.* **17** 2603
- [53] Decher G and Schlenoff J B (ed) 2003 *Multilayer Thin Films* (Weinheim: Wiley-VCH)
- [54] Serpe J S, Kim J and Lyon L A 2004 *Adv. Mater.* **16** 184
- [55] Kim J, Serpe J S and Lyon L A 2004 *J. Am. Chem. Soc.* **126** 9512
- [56] Kim J, Serpe J S and Lyon L A 2005 *Angew. Chem. Int. Edn* **44** 1333
- [57] Konieczny M and Likos C N 2007 *Soft Matter* **3** 1130
- [58] Jusufi A, Konieczny M and Likos C N 2008 in preparation
- [59] Bianchi E, Largo J, Tartaglia P, Zaccarelli E and Sciortino F 2006 *Phys. Rev. Lett.* **97** 168301
- [60] Corezzi S, De Michele C, Zaccarelli E, Fioletto D and Sciortino F 2008 *Soft Matter* **4** 1173
- [61] Grest G S 1994 *Macromolecules* **27** 3493
- [62] Coluzza I and Hansen J P 2008 *Phys. Rev. Lett.* **100** 016104
- [63] Milner S T, Witten T A and Cates M E 1988 *Macromolecules* **21** 2610
- [64] Netz R R and Schick M 1998 *Macromolecules* **31** 5105
- [65] Seidel C and Netz R R 2000 *Macromolecules* **33** 634
- [66] Fazli H, Golestanian R, Hansen P L and Kolahchi M R 2006 *Europhys. Lett.* **73** 429
- [67] Jusufi A, Likos C N and Ballauff M 2004 *Colloid. Polym. Sci.* **282** 910
- [68] Dubois M, Schönhoff M, Meister A, Belloni L, Zemb T and Möwald H 2006 *Phys. Rev. E* **74** 051402
- [69] Kegler K, Salomo M and Kremer F 2007 *Phys. Rev. Lett.* **98** 058304

- [70] Kegler K, Konieczny M, Dominguez-Espinoza G, Gutsche C, Salomo M, Kremer F and Likos C N 2008 *Phys. Rev. Lett.* **100** 118302
- [71] Kornyshev A K, Lee D J, Leikin S and Wynveen A 2007 *Rev. Mod. Phys.* **79** 943
- [72] Saenger W 1984 *Principles of Nucleic Acid Structure* (New York: Springer)
- [73] Berman H M, Olson W K, Beveridge D L, Westbrook J, Gelbin A, Demeny A, Hsieh S-H, Srinivasan A R and Schneider B 1992 *Biophys. J.* **63** 751
- [74] Wynveen A, Lee D J, Kornyshev A A and Leikin S 2008 *Nucl. Acids Res.* at press doi:10.1093/nar/gkn514
- [75] Terao T 2002 *Phys. Rev. E* **66** 046707
- [76] Crozier P S and Stevens M J 2003 *J. Chem. Phys.* **118** 3855